Journal of Alloys and Compounds 282 (1999) 164–174

Study of the Ag–In–Te ternary system I. Description of the triangle Ag_2Te–In_2Te_3–Te

Zahra Bahari[a], Jacques Rivet[a], Bernard Legendre[b], Jérôme Dugué[a,*]

[a]Laboratoire de Chimie Physique et de Chimie Minérale Structurale, Faculté des Sciences Pharmaceutiques et Biologiques, Université René-Descartes, 4, Avenue de l'Observatoire, 75270 Paris Cedex 06, France

[b]Laboratoire de Chimie Physique Minérale et Bioinorganique (E.A. 401), Faculté des Sciences Pharmaceutiques et Biologiques, Université Paris XI, Rue J.-B. Clément, 92296 Châtenay-Malabry Cedex, France

Received 18 August 1998

Abstract

The phase diagram of the Ag_2Te–In_2Te_3–Te system was studied by DTA, DSC and XRD methods. Three ternary phases are observed in the quasi-binary Ag_2Te–In_2Te_3 section: $AgIn_5Te_8$, which presents a congruent melting point at 725°C and a solid–solid transition at 699°C, with tetragonal structure for the two varieties; $Ag_3In_{97}Te_{147}$, which presents a cubic structure, melts incongruently at 672°C; $AgInTe_2$, which crystallizes in a chalcopyrite-type structure at room temperature, undergoes a solid–solid transition at 410/475°C and a binary peritectic decomposition at 650°C. The eutectic valleys are drawn, and the nature and the location of the ternary invariants are given. Eight ternary invariants were found: two ternary eutectics points, five transitory ternary peritectic points and one metatectic point. No liquid–liquid miscibility gap and no glassy region are observed.

Keywords: Phase diagrams; Binary systems; Ternary systems; Liquid–solid equilibria; Silver indium tellurides

1. Introduction

Ternary silver chalcogenide glasses are known to present ionic conductivity. In order to find glassy regions, when chalcogen is tellurium, we have previously investigated, in a series of papers, the Ag–M–Te ternary phase diagrams, where M=Ga [1], Ge [2] and As [3].

No thermal study has been thoroughly realized of the ternary Ag–In–Te system. Therefore, we found it interesting to devote a study to this system in order to determine the composition of the different crystalline phases and that of the ternary invariants, the traces of the eutectic valleys and the regions of liquid–liquid miscibility gaps originating from the binary systems Ag–Te and In–Te.

The Ag_2Te–In_2Te_3 section has earlier been studied [4–6]. However, the authors disagree about the numbers and the compositions of phases which exist on this line. They agree about the existence of the phase $AgInTe_2$.

As the Ag_2Te–In_2Te_3 section is a quasi-binary one, the Ag–In–Te system can be divided by this section into two independent sub-systems: a triangle, Ag_2Te–In_2Te_3–Te, and a quadrilateral, Ag–Ag_2Te–In_2Te_3–In. In this paper, we report the results obtained for the triangle. Our study lends support to the existence of three ternary compounds: one, $AgIn_5Te_8$, which melts congruently, and two, $Ag_3In_{97}Te_{147}$ and $AgInTe_2$, which undergo peritectic decompositions. We could not identify any ternary liquid–liquid miscibility gap or glassy region. A study of the quadrilateral Ag–Ag_2Te–In_2Te_3–In will be presented in a following paper [7].

2. Materials and methods

The ternary Ag–In–Te system was studied by differential thermal analysis (DTA), differential scanning calorimetry (DSC) and X-ray diffraction (XRD) methods.

The differential thermal analyzer included a furnace and a Netzsch autotimer associated to a Linseis recorder. The thermocouples used were made of Pt–Pt (10% Rh). The heating rate was 5°C min^{-1}. The analyzer was standardized by the fusion temperatures of the elements: Ag, T_f=962°C; Zn, T_f=420°C; and Sn, T_f=232°C. To realize the differential calorimetric analysis we used a DSC Setaram 111 at a heating rate of 1°C min^{-1}. Calibrations

*Corresponding author. Tel.: +33-1-53739668; fax: +33-1-43290592; e-mail: dugue@pharmacie.univ-paris5.fr

0925-8388/99/$ – see front matter
PII: S0925-8388(98)00839-1

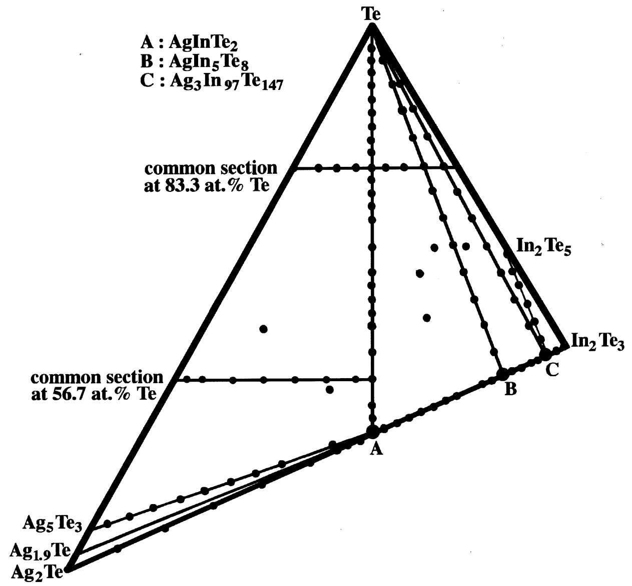

Fig. 1. Triangulation of the Ag_2Te–In_2Te_3–Te system (black dots represent compositions studied).

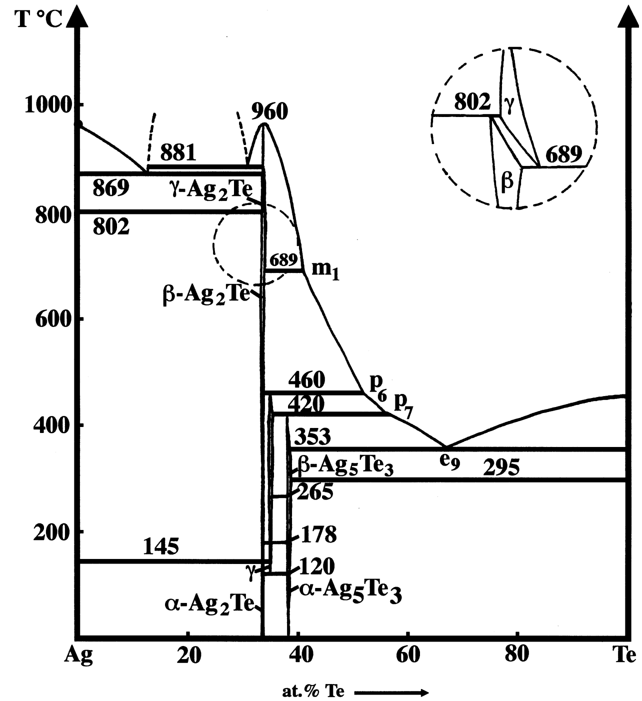

Fig. 2. Phase diagram of the Ag–Te binary system according to Kracek et al. [8].

were performed by the elements: Sb, $T_f=631$°C; Pb, $T_f=328$°C; Sn, $T_f=232$°C; and In, $T_f=157$°C.

The X-ray diffraction studies of ground samples were performed at room temperature by a CGR diffractometer using the radiation Cu Kα. At a variable temperature, studies were performed with a Guinier-Lenné's camera using the Seemann–Bohlin geometric arrangement.

The primary materials used had the following purity grade: Ag and Te 99.999%; In 99.99%. Blendings of these elements in small blocks or in wires were introduced into an evacuated (10^{-3} Torr) silica ampoule. The preparations were thereafter put in a muffle furnace where they were progressively heated up to 1000°C. They remained at this temperature for 18 h to favor a complete combination of the elements and to give homogenous alloys. Then, they were either slowly cooled or annealed at a suitable temperature for a month or even longer. More than 100 syntheses have been realized (Fig. 1).

3. Bibliographic data on the binary systems

3.1. The Ag–Te binary system (Fig. 2)

Fig. 2 shows that the system Ag–Te [8] has two eutectics, the first one at a temperature of 353°C with a content of 66.7 at.% Te, the second one at a temperature of 869°C with a content of 12.5 at.% Te. This system also contains a liquid–liquid miscibility gap between the compositions 13.5 and 30.3 at.% Te. The monotectic invariant has a temperature of 881°C.

This binary system presents three phases: (1) Ag_2Te, with a congruent melting point at 960°C, presents two phase transitions: the first one at 145°C ($\alpha \rightleftarrows \beta$) and the second one at 689/802°C ($\beta \rightleftarrows \gamma$); the β and the γ phases present solid miscibility regions. At 689°C, the γ phase is characterized by the following binary metatectic reaction (formulas of phases written in brackets correspond to solid miscibility regions):

$$\text{Liq } m_1 + \langle \beta Ag_2Te \rangle \rightleftarrows \langle \gamma Ag_2Te \rangle$$

(2) $Ag_{1.9}Te$, 'γ phase', is stable in the interval from 120 to 460°C with a peritectic decomposition and undergoes a transition at 178°C; (3) Ag_5Te_3 also presents a peritectic decomposition at 420°C with a transition at 265/295°C.

3.2. The In–Te binary system (Fig. 3)

Our results correspond to the phase diagram described by Grochowski et al. [9]. However, we could not confirm the existence of the In_3Te_5 phase.

This binary system shows a eutectic at 427°C, with a composition of 88 at.% Te and a monotectic invariant at 423°C linked with the presence of a liquid–liquid miscibility gap between the compositions 2.3 and 27.6 at.% Te.

To confirm the nature of the invariant which exists in the zone rich in indium we used the DSC method which is more precise and more sensitive at low thermal effects than the DTA method. Indeed, the invariant is located at the temperature of 157.4°C that is higher than the melting

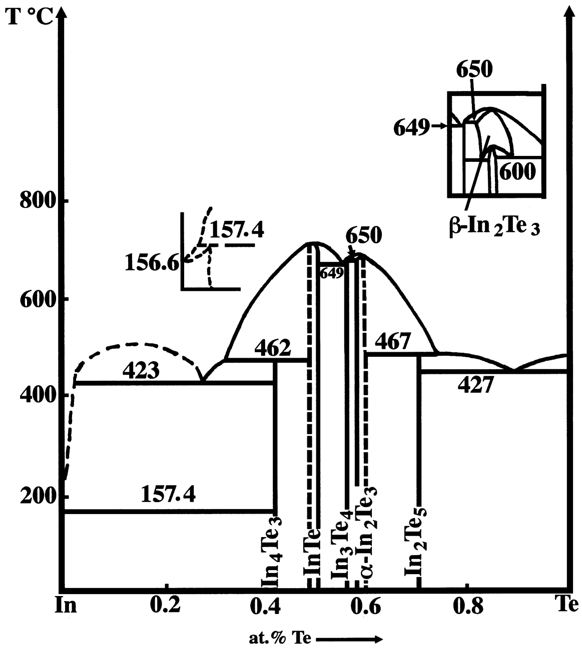

Fig. 3. Phase diagram of the In–Te binary system.

point of indium (156.63°C). The invariant shows a peritectic reaction.

This binary system contains several phases, In_3Te_4, In_2Te_5 and In_4Te_3 with peritectic decompositions at 650, 467 and at 462°C, respectively. Two other phases InTe and In_2Te_3 melt congruently at 696 and at 667°C, respectively.

3.3. The Ag_2Te–In_2Te_3 section (Fig. 4)

The phase diagram of the Ag_2Te–In_2Te_3 system has been described by Chiang et al. [4]. They showed the existence of four compounds: $AgIn_3Te_5$ which melts congruently at 699°C and presents a large solid miscibility region; $AgIn_9Te_{14}$, $Ag_3In_{37}Te_{57}$ and $AgInTe_2$ which undergo peritectic decompositions at 694, 686 and 658°C, respectively. These authors attributed chalcopyrite-type structures to the three compounds $AgIn_3Te_5$, $AgIn_9Te_{14}$ and $AgInTe_2$.

Mayet and Roubin [5] studied the same system but limited their study to the interval between $AgInTe_2$ and In_2Te_3. They confirmed the existence and the structure type of $AgInTe_2$ and $AgIn_9Te_{14}$ and identified a new phase, $Ag_3In_{97}Te_{147}$, which crystallizes in the c.f.c. system. However, they did not obtain evidence for the existence of the congruent phase $AgIn_3Te_5$.

Palatnik and Rogacheva [6] disagreed with these conclusions and obtained only evidence for the existence of $AgInTe_2$. They also found a new compound $AgIn_5Te_8$.

We have recently resumed the study of this same section [10] and we confirmed the existence of the three ternary compounds (Fig. 4): (1) $AgIn_5Te_8$, which melts congruently at 725°C and which presents a large miscibility region. Thus, we lend support to the result of Palatnik and Rogacheva [6]; (2) $Ag_3In_{97}Te_{147}$ (found by Chiang et al. [4]) which melts incongruently at 672°C and which presents a cubic structure; (3) $AgInTe_2$ (found by Chiang et al. [4], by Mayet and Roubin [5] and by Palatnik and Rogacheva [6]) which melts incongruently at 650°C and which presents a chalcopyrite-type structure with a miscibility region. However, we could not find any evidence for the existence of the compounds $AgIn_3Te_5$, $Ag_3In_{37}Te_{57}$ and $AgIn_9Te_{14}$ proposed by Chiang et al. [4]. Table 1 gives the phase equilibria in the regions spanned by the Ag_2Te–In_2Te_3 section.

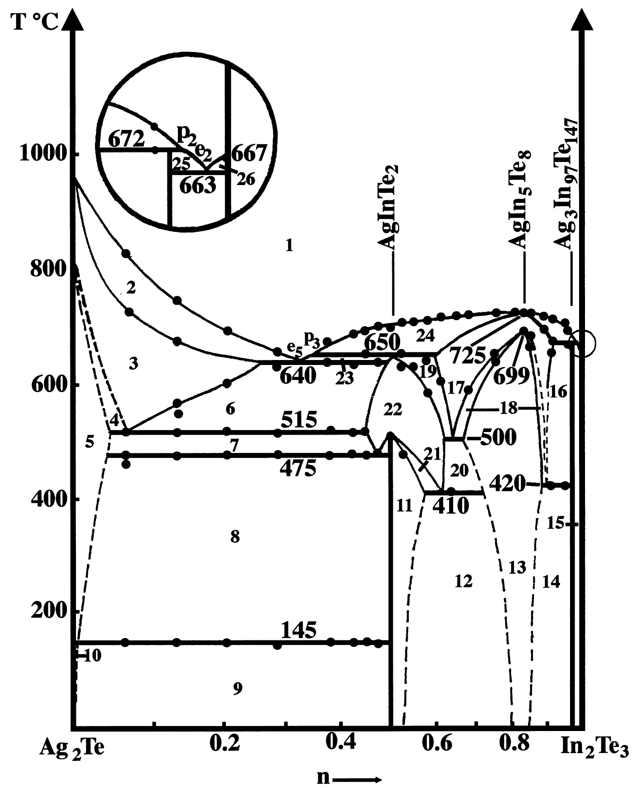

Fig. 4. Phase diagram of the Ag_2Te–In_2Te_3 quasi-binary section.

4. The Ag_2Te–In_2Te_3–Te ternary system

4.1. Triangulation of the system (Fig. 1)

The triangulation is achieved at room temperature by an X-ray diffraction analysis of samples obtained by slow cooling. As Ag_2Te, In_2Te_3 and $AgIn_5Te_8$ melt congruently, Ag_2Te–In_2Te_3 and $AgIn_5Te_8$–Te are quasi-binary sections which define two subternary systems. We obtained thus evidence for two sub-ternaries: (1) In_2Te_3–$AgIn_5Te_8$–Te, which contains three secondary triangles, (2) Ag_2Te–Te–$AgIn_5Te_8$, which contains four triangles of invariance. Except the two common sections the lines in Fig. 1, which are either invariant or quasi-binaries lines, are defined by the Guertler method [11].

Table 1
Phase equilibria in the regions contained in the Ag_2Te–In_2Te_3 section

Region number	Phases
1	L
2	$L+\langle\gamma Ag_2Te\rangle$
3	$\langle\gamma Ag_2Te\rangle$
4	$\langle\gamma Ag_2Te\rangle+\langle\beta Ag_2Te\rangle$
5	$\langle\beta Ag_2Te\rangle$
6	$\langle\gamma Ag_2Te\rangle+\langle\beta AgInTe_2\rangle$
7	$\langle\beta Ag_2Te\rangle+\langle\beta AgInTe_2\rangle$
8	$\langle\beta Ag_2Te\rangle+\langle\alpha AgInTe_2\rangle$
9	$\langle\alpha Ag_2Te\rangle+\langle\alpha AgInTe_2\rangle$
10	$\langle\alpha Ag_2Te\rangle$
11	$\langle\alpha AgInTe_2\rangle$
12	$\langle\alpha AgInTe_2\rangle+\langle\alpha AgIn_5Te_8\rangle$
13	$\langle\alpha AgIn_5Te_8\rangle$
14	$\langle\alpha AgIn_5Te_8\rangle+Ag_3In_{97}Te_{147}$
15	$Ag_3In_{97}Te_{147}+In_2Te_3$
16	$\langle\beta AgIn_5Te_8\rangle+Ag_3In_{97}Te_{147}$
17	$\langle\beta AgIn_5Te_8\rangle$
18	$\langle\alpha AgIn_5Te_8\rangle+\langle\beta AgIn_5Te_8\rangle$
19	$\langle\beta AgIn_5Te_8\rangle+\langle\beta AgInTe_2\rangle$
20	$\langle\beta AgInTe_2\rangle+\langle\alpha AgIn_5Te_8\rangle$
21	$\langle\alpha AgInTe_2\rangle+\langle\beta AgInTe_2\rangle$
22	$\langle\beta AgInTe_2\rangle$
23	$L+\langle\beta AgInTe_2\rangle$
24	$L+\langle\beta AgIn_5Te_8\rangle$
25	$L+Ag_3In_{97}Te_{147}$
26	$L+In_2Te_3$

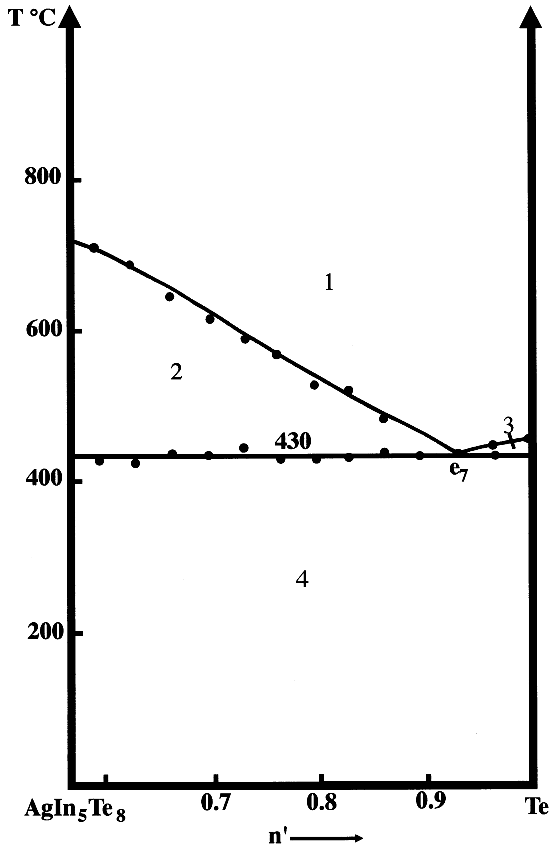

Fig. 5. Phase diagram of the $AgIn_5Te_8$–Te quasi–binary section.

In the text below the compositions are indicated by atomic ratios: $n=In/(In+Ag)$ or $n'=Te/(Ag+In+Te)$.

4.2. The $AgIn_5Te_8$–Te quasi-binary section (Fig. 5)

Fig. 5 shows that two liquidus curves converge on the line located at 430°C at the point e_7 ($n'=0.93$). As the peritectic valley U_2U_5 crosses the $AgIn_5Te_8$–Te section, at its temperature maximum, the eutectic point e_7 is a saddle point (Fig. 13). Further, as this section is adjacent to an element and to a congruent melting compound it is a quasi-binary section. Table 2 gives the phase equilibria in the regions located in this section.

4.3. The $Ag_3In_{97}Te_{147}$–Te section (Fig. 6)

Fig. 6 shows that, at 424°C, the liquidus curve has its minimum point, α_2, with a composition $n'=0.9$. The eutectic valley originating from e_7 decreases into the triangle In_2Te_3–$Ag_3In_{97}Te_{147}$–Te and goes further towards the ternary peritectic U_2 located at 420°C (Fig. 13). The point ϵ_2 is the trace of the minimal tie line originating from $AgIn_5Te_8$ and going towards U_2 (Table 3).

4.4. The $Ag_3In_{97}Te_{147}$–In_2Te_5 section (Fig. 7)

This section is bounded by two compounds which undergo peritectic decompositions, In_2Te_5 and $Ag_3In_{97}Te_{147}$. Even if this section is a restricted region, it is of high interest as it can confirm the laying out of the valleys and the temperatures of the ternary invariants (Fig. 13).

Three characteristic isothermal lines are observed. The first one, at 412°C, corresponds to the temperature of the ternary eutectic E_1 equilibrium:

$$\text{Liq. } E_1 \rightleftarrows Te + In_2Te_5 + Ag_3In_{97}Te_{147}$$

The second one, at 420°C, corresponds to the transitory ternary peritectic invariant U_2:

$$\text{Liq. } U_2 + AgIn_5Te_8 \rightleftarrows Ag_3In_{97}Te_{147} + Te$$

The third one, at 445°C, corresponds to the transitory ternary peritectic U_1:

$$\text{Liq. } U_1 + In_2Te_3 \rightleftarrows In_2Te_5 + Ag_3In_{97}Te_{147}$$

Between the melting points of $Ag_3In_{97}Te_{147}$ and In_2Te_5

Table 2
Phase equilibria in the regions contained in the $AgIn_5Te_8$–Te section

Region number	Phases
1	L
2	$L+AgIn_5Te_8$
3	$L+Te$
4	$Te+AgIn_5Te_8$

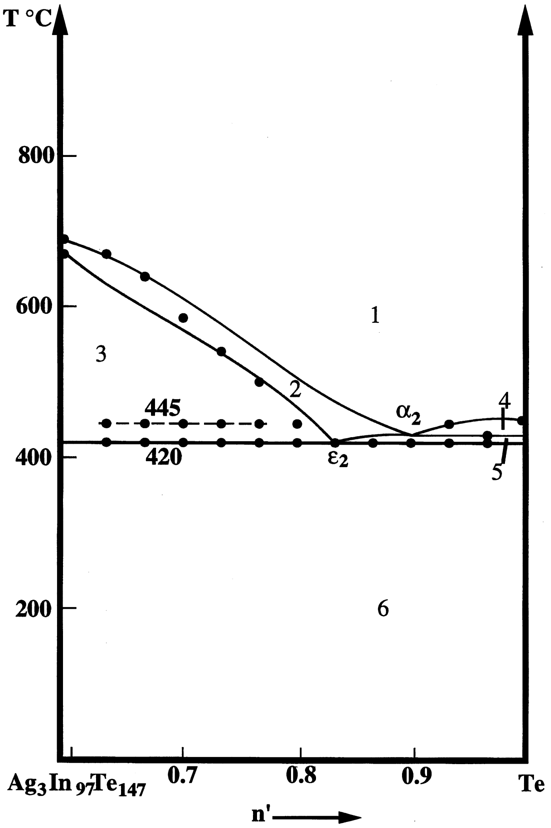

Fig. 6. Phase diagram of the $Ag_3In_{97}Te_{147}$–Te section.

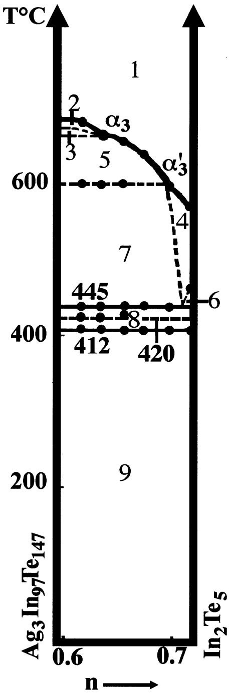

Fig. 7. Phase diagram of the $Ag_3In_{97}Te_{147}$–In_2Te_5 section.

the liquidus curve decreases continuously with two discontinuities at α_3, 670°C, and at α'_3, 600°C. The first one, at point α_3, at 670°C, corresponds to the crossing of the valley originating from p_2 going towards U_2 (Fig. 13). The second one, at point α'_3, at 600°C, corresponds to the crossing of the valley originating from the quasi-binary eutectic e_2 and going towards the ternary peritectic U_1 (Table 4).

4.5. The $AgInTe_2$–Te section (Fig. 8)

Two isothermal lines appear on this section. The first one, at 350°C, corresponds to the temperature of the ternary eutectic E_2 equilibrium:

$$\text{Liq. } E_2 \rightleftarrows \text{Te} + Ag_5Te_3 + \langle \alpha AgInTe_2 \rangle$$

The second one, at 390°C, corresponds to the transitory ternary peritectic U_5 equilibrium:

$$\text{Liq. } U_5 + \langle AgIn_5Te_8 \rangle \rightleftarrows \langle AgInTe_2 \rangle + \text{Te}$$

The liquidus curves converge on point α_1 located at 400°C, $n' = 0.89$. This point, α_1, corresponds to the crossing of the valley originating from e_7 and going down towards the transitory ternary peritectic U_5 (Fig. 13). At the point ϵ_1 the section cuts the minimal tie-line originating from $AgIn_5Te_8$ which goes through U_5. The line $AgInTe_2$–Te is bounded on one side by the compound $AgInTe_2$, which undergoes a peritectic decomposition, and on the other side by the element Te. Thus, this line is not a quasi-binary line but an invariant line. Further, the X-ray diffraction analysis carried out on samples along this line gave mixtures of only these two extreme phases.

The slight extension of the miscibility region near

Table 3
Phase equilibria in the regions contained in the $Ag_3In_{97}Te_{147}$–Te section

Region number	Phases
1	L
2	$L + AgIn_5Te_8$
3	$L + AgIn_5Te_8 + Ag_3In_{97}Te_{147}$
4	L + Te
5	$L + AgIn_5Te_8 + Te$
6	$Te + Ag_3In_{97}Te_{147}$

Table 4
Phase equilibria in the regions contained in the $Ag_3In_{97}Te_{147}$–In_2Te_5 section

Region number	Phases
1	L
2	$L + AgIn_5Te_8$
3	$L + AgIn_5Te_8 + Ag_3In_{97}Te_{147}$
4	$L + In_2Te_3$
5	$L + Ag_3In_{97}Te_{147}$
6	$L + In_2Te_3 + In_2Te_5$
7	$L + In_2Te_3 + Ag_3In_{97}Te_{147}$
8	$Ag_3In_{97}Te_{147} + In_2Te_5 + In_2Te_3$
9	$Ag_3In_{97}Te_{147} + In_2Te_5$

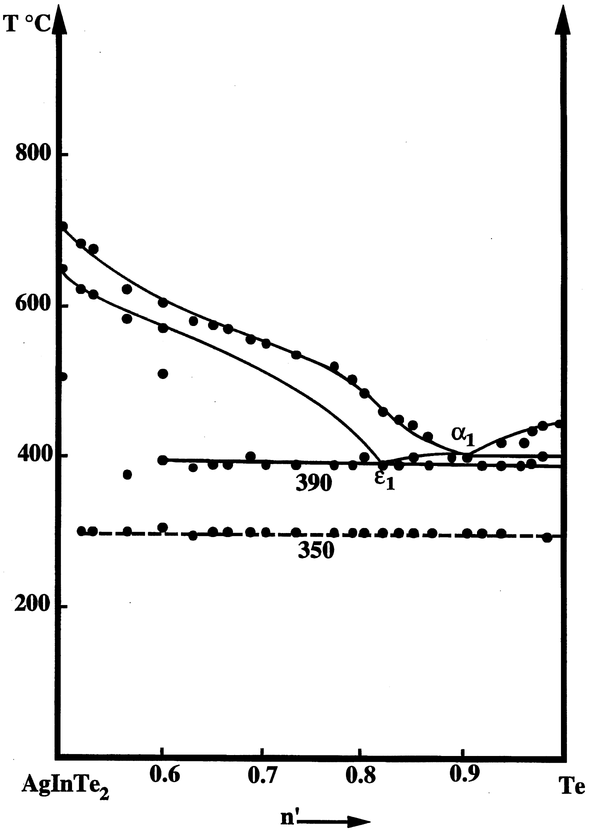

Fig. 8. Phase diagram of the $AgInTe_2$–Te section.

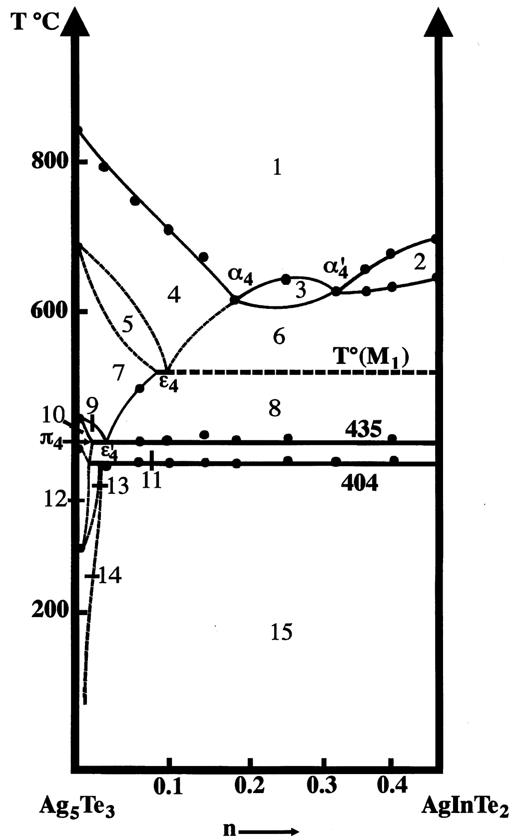

Fig. 9. Phase diagram of the Ag_5Te_3–$AgInTe_2$ section (dotted lines represent theoretical lines).

$AgInTe_2$ on both sides of the Ag_2Te–In_2Te_3 section made it very difficult to give a complete interpretation of the region rich in $AgInTe_2$. The DTA analysis did not show any ternary solid–solid transitions in spite of a large number of experiments.

4.6. The Ag_5Te_3–$AgInTe_2$ section (Fig. 9)

This section is bound by the two compounds, Ag_5Te_3 and $AgInTe_2$, which undergo incongruent melting at 420°C and 650°C, respectively. This invariant section gives us the temperatures of the two ternary invariants U_3 and U_4. The first one, at 435°C, U_3, is the ternary transitory peritectic invariant of the triangle Ag_2Te–$Ag_{1.9}Te$–$AgInTe_2$:

$$\text{Liq. } U_3 + \langle \beta Ag_2Te \rangle \rightleftarrows Ag_{1.9}Te + \langle AgInTe_2 \rangle$$

The second one, at 404°C, U_4, is the ternary transitory peritectic invariant of the triangle $Ag_{1.9}Te$–Ag_5Te_3–$AgInTe_2$:

$$\text{Liq. } U_4 + Ag_{1.9}Te \rightleftarrows Ag_5Te_3 + \langle AgInTe_2 \rangle$$

As a binary metatectic point m_1 exists in the binary Ag–Te system, it constrains the existence of a ternary metatectic point M_1 with the equilibrium:

$$\text{Liq. } M_1 + \langle \gamma Ag_2Te \rangle \rightleftarrows \langle \beta Ag_2Te \rangle + \langle AgInTe_2 \rangle$$

But the ternary solid–solid transitions of Ag_2Te were not observed, so the temperature of M_1 could not be exactly determined. However, this temperature must be located between the temperatures of the point α_4 and that of the point U_3: $435°C < T(M_1) < 620°C$.

The valley originating from e_5 at 640°C crosses this section at point α_4 (620°C) and continues its descent down to M_1 (Fig. 13). At the point ϵ_4 the section cuts the minimal tie-line originating from $\langle \gamma Ag_2Te \rangle$, which goes through M_1. Owing to the uncertainty in composition and in temperature of M_1, we cannot exactly localize the point ϵ_4. At the point ϵ'_4 (435°C) the section cuts the minimal tie-line originating from $\langle \beta Ag_2Te \rangle$ and going through U_3. At the point π_4 (435°C), the section cuts the edge of $Ag_{1.9}Te$–U_3 which corresponds to the invariant plane U_3 (Fig. 12). The peritectic valley originating from p_3 (650°C) crosses this section at point α'_4 (630°C) and ends at U_5 (390°C).

On account to the uncertainty of the temperature of M_1, on the one hand, and of the solid–solid transition of $\langle Ag_5Te_3 \rangle$, on the other hand the drawing of Fig. 9 is partly theoretical. Furthermore, the miscibility regions of both solid varieties of $AgInTe_2$ have been omitted in this figure. Table 5 gives the phase equilibria in the regions contained in this section.

Table 5
Phase equilibria in the regions contained in the Ag_5Te_3–$AgInTe_2$ section

Region number	Phases
1	L
2	$L+\langle\beta\ AgIn_5Te_8\rangle$
3	$L+\langle\beta AgInTe_2\rangle$
4	$L+\langle\gamma Ag_2Te\rangle$
5	$L+\langle\gamma Ag_2Te\rangle+\langle\beta Ag_2Te\rangle$
6	$L+\langle\gamma Ag_2Te\rangle+\langle\beta AgInTe_2\rangle$
7	$L+\langle\beta Ag_2Te\rangle$
8	$L+\langle\beta Ag_2Te\rangle+\langle\alpha AgInTe_2\rangle$
9	$L+\langle\beta Ag_2Te\rangle+Ag_{1.9}Te$
10	$L+Ag_{1.9}Te$
11	$L+Ag_{1.9}Te+\langle\alpha AgInTe_2\rangle$
12	$\langle\beta Ag_5Te_3\rangle$
13	$\langle\beta Ag_5Te_3\rangle+\langle\alpha Ag_5Te_3\rangle$
14	$\langle\alpha Ag_5Te_3\rangle$
15	$\langle\alpha Ag_5Te_3\rangle+\langle\alpha AgInTe_2\rangle$

4.7. The common section at 83.3 at.% Te ($Ag_{1.67}Te_{8.33}$–$In_{1.67}Te_{8.33}$) (Fig. 10)

A study of a section near U_5 is necessary for the drawing of the eutectic valley e_7E_2, which stretches down passing through α_1 (Fig. 13). This section has two crossings, the first one at α_5 (378°C) and the second one at α'_5 (445°C). The point α_5 corresponds to the crossing of the eutectic valley U_5E_2.

From Te originate two ruled surfaces which are bounded by the eutectic valleys e_9E_2 and U_5E_2. As the temperature decreases the section cuts the liquidus surfaces and produces the curves $\epsilon_5 t$ and $\epsilon_5\alpha_5$. At the point ϵ_5 the section cuts the minimal tie line originating from Te which goes through E_2. The point α'_5 corresponds to the crossing of the eutectic valley p_3U_5.

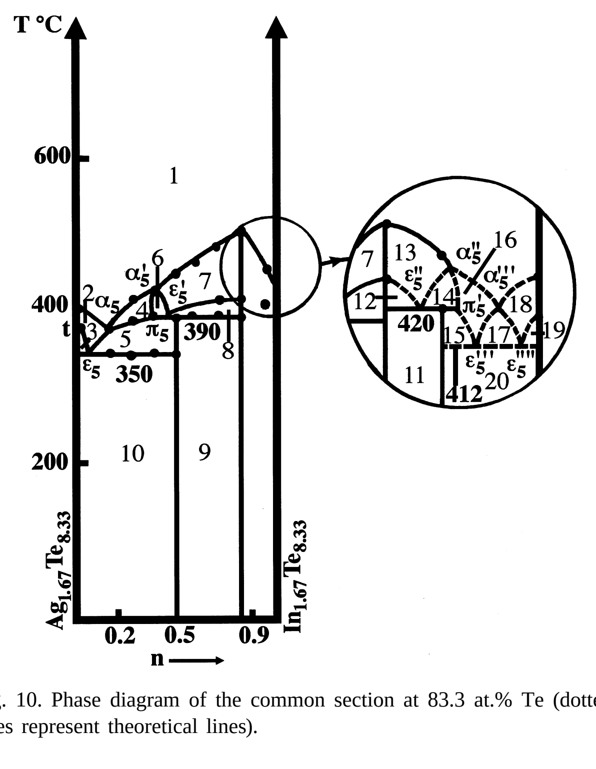

Fig. 10. Phase diagram of the common section at 83.3 at.% Te (dotted lines represent theoretical lines).

The section cuts four invariant planes: two eutectic planes E_1 and E_2 at 412 and 350°C, respectively, and two peritectic planes U_2 and U_5 at 420 and 390°C, respectively.

At the point ϵ'_5 the section cuts the minimal tie line originating from $AgIn_5Te_8$ which goes through U_5. At the point π_5 the section cuts the edge $AgInTe_2$–U_5 which corresponds to the invariant plane U_5 (Fig. 12).

As the liquidus shows a maximum at $n=0.83$ it confirms the quasi-binary type of the $AgIn_5Te_8$–Te section. As the region $0.83<n<1$ is very restricted experimental interpretation becomes more difficult. Therefore, the drawing in the magnification which we show in Fig. 10 is theoretical. This drawing is justified from the necessary existence of the crossing of two valleys, the first one p_2U_2 at α''_5 passing towards the ternary peritectic U_2, and the second one U_1E_1 at α'''_5 passing towards the ternary eutectic E_1. Between α'''_5, which is the crossing of the traces of the two liquidus surfaces, and the ternary eutectic plane E_1, at 412°C, traces are given of four ruled surfaces, which define three three-phase regions (regions 15, 17 and 19, Fig. 10).

At the point ϵ''_5 the section cuts the minimal tie line originating from $AgIn_5Te_8$ which goes through U_2. At the point π'_5 the section cuts the edge $Ag_3In_{97}Te_{147}$–U_2 which corresponds to the invariant plane U_2. The two points ϵ'''_5 and ϵ''''_5 correspond to the intersection of the minimal tie lines originating from the compounds $Ag_3In_{97}Te_{147}$ and In_2Te_5, respectively. They are both going towards E_1. Table 6 gives the phase equilibria in the regions contained in this section.

Table 6
Phase equilibria in the regions contained in the section at 83.3 at.% Te

Region number	Phases
1	L
2	$L+Ag_5Te_3$
3	$L+Ag_5Te_3+Te$
4	$L+AgInTe_2$
5	$L+AgInTe_2+Ag_5Te_3$
6	$L+AgInTe_2+Te$
7	$L+AgIn_5Te_8$
8	$L+AgIn_5Te_8+Te$
9	$AgInTe_2+AgIn_5Te_8+Te$
10	$AgInTe_2+Ag_5Te_3+Te$
11	$AgIn_5Te_8+Ag_3In_{97}Te_{147}+Te$
12	$L+AgIn_5Te_8+Te$
13	$L+AgIn_5Te_8$
14	$L+Ag_3In_{97}Te_{147}+AgIn_5Te_8$
15	$L+Ag_3In_{97}Te_{147}+Te$
16	$L+Ag_3In_{97}Te_{147}$
17	$L+Ag_3In_{97}Te_{147}+In_2Te_5$
18	$L+In_2Te_5$
19	$L+In_2Te_5+Te$
20	$Ag_3In_{97}Te_{147}+In_2Te_5+Te$

4.8. The common section at 56.7 at.% Te ($Ag_{4.33}Te_{5.67}$–$Ag_{2.17}In_{2.17}Te_{5.67}$) (Fig. 11)

A study of a section between p_6 and p_7 is necessary for the drawings of the two valleys e_5E_2 and p_3U_5 (Fig. 13). It confirms the compositions of the ternary invariants U_4 and E_2 which are found in the triangle Te–Ag_2Te–$AgInTe_2$. At the points ϵ_6 and ϵ'_6 the section cuts two minimal tie lines. The first one originates from Ag_5Te_3 and goes towards E_2. The second one originates from $Ag_{1.9}Te$ and goes towards U_4.

At the points π_6 and π'_6 the section cuts the edges of the two sections Ag_5Te_3–U_4 and $AgInTe_2$–U_4, respectively, which correspond to the invariant plane U_4 (Figs. 12 and 13).

At 427°C the eutectic valley originating from the binary eutectic point e_5 crosses the section at point α_6 on its way down to the ternary transitory peritectic invariant U_4 at 404°C (equilibrium given in Section 4.6). The point α'_6, at 600°C, corresponds to the crossing of the eutectic valley originating from the binary peritectic point p_3 going to the ternary peritectic U_5 (Fig. 12).

The point ϵ''_6 is the crossing of the minimal tie line originating from $AgInTe_2$ going towards E_2. Table 7 gives the phase equilibria in the regions contained in this section.

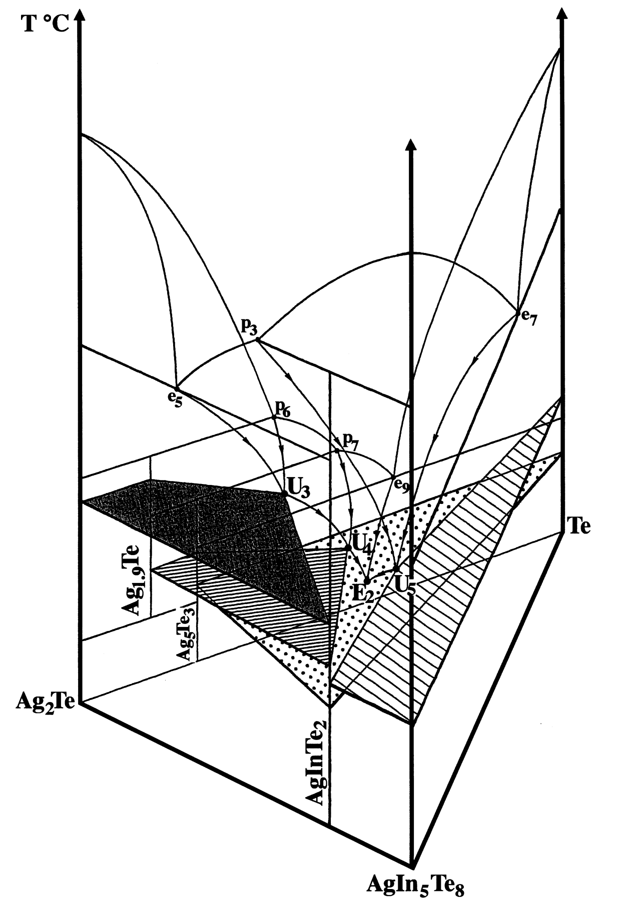

Fig. 12. Space view of the $AgIn_5Te_8$–Ag_2Te–Te sub-ternary system showing the invariant planes.

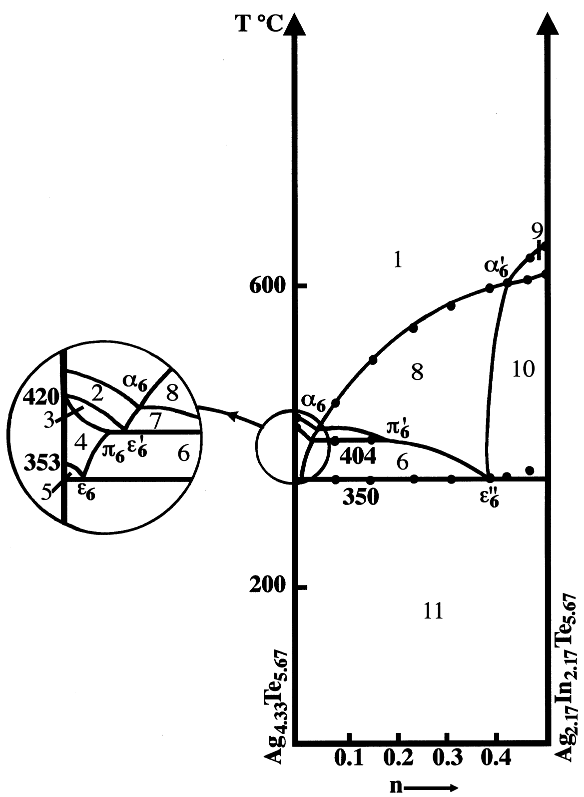

Fig. 11. Phase diagram of the common section at 56.7 at.% Te.

5. The evolution of the solid–liquid equilibria (Fig. 14)

The two valleys originating from the binary eutectic point e_2 (663°C) and from the binary peritectic point p_4 (467°C) decrease and join each other at the transitory peritectic point U_1, where they give, at 445°C, the equilibrium already presented in Section 4.4.

The two valleys originating from the binary peritectic point p_2 (672°C) and from the quasi-binary eutectic point e_7 (430°C) meet each other at the peritectic point U_2 (420°C) (equilibrium given in Section 4.4).

The eutectic valley originating from e_8 (427°C) meets at E_1 (412°C) the two valleys which come from the two peritectic points U_1 and U_2 (equilibrium given in Section 4.4).

The two valleys originating from the binary metatectic point m_1 (689°C) and from the binary eutectic point e_5 (640°C) join each other at the metatectic point M_1 (equilibrium given in Section 4.4).

The two valleys originating from the ternary metatectic point M_1 and from the binary peritectic point p_6 (460°C) join each other at the peritectic point U_3 (435°C) (equilibrium given in Section 4.6).

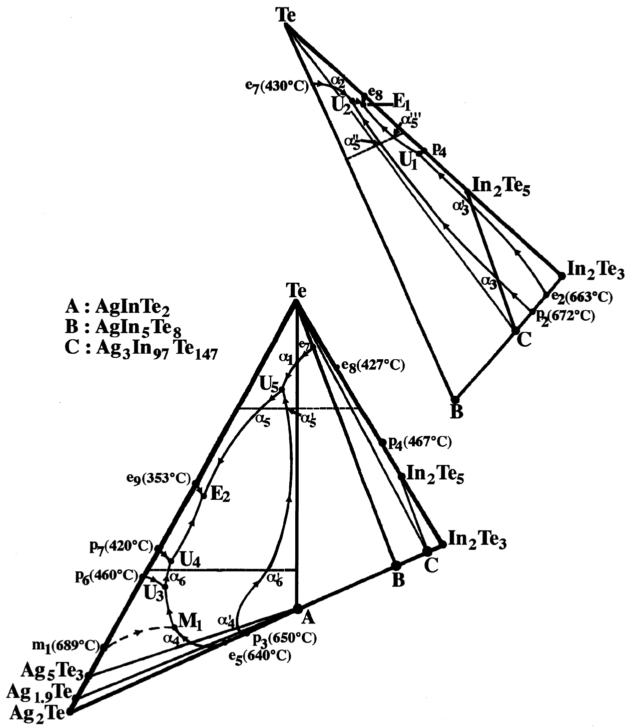

Fig. 13. Phase diagram of the Ag_2Te–In_2Te_3–Te ternary system.

The two valleys originating from the peritectic point U_3 and from the binary peritectic point p_7 (420°C) join each other at the peritectic point U_4 (404°C) (equilibrium given in Section 4.6).

The two valleys originating from the binary peritectic point p_3 (650°C) and from the quasi-binary eutectic point e_7 (430°C) join each other at the peritectic point U_5 (390°C) (equilibrium given in Section 4.5).

The eutectic valley originating from the binary eutectic point e_9 (353°C) meets at E_2 (350°C) two valleys which come from the two peritectic points U_4 and U_5 (equilibrium given in Section 4.5).

Fig. 14 shows the evolution of the solid–liquid equilibria in the two triangles Ag_2Te–$AgInTe_2$–Te and $AgInTe_2$–In_2Te_3–Te. Below we give four solid–solid equilibria in the Ag_2Te–In_2Te_3 quasi-binary section which are not included in Fig. 14. As mentioned in Section 4.5 and Section 4.6 the existence of miscibility regions for Ag_2Te, $AgInTe_2$ and Ag_5InTe_8 made it very difficult to give a complete interpretation of the solid-state reactions. Thus, for these equilibria we cannot give the connections with the ternary solid–solid equilibria.

$$\langle \gamma Ag_2Te \rangle \rightleftarrows \langle \beta Ag_2Te \rangle + \langle \beta AgInTe_2 \rangle \quad \text{at } 515°C$$

$$\langle \beta AgIn_5Te_8 \rangle \rightleftarrows \langle \alpha AgIn_5Te_8 \rangle + \langle \beta AgInTe_2 \rangle \quad \text{at } 500°C$$

$$\langle \beta AgInTe_2 \rangle \rightleftarrows \langle \beta Ag_2Te \rangle + \langle \alpha AgInTe_2 \rangle \quad \text{at } 475°C$$

$$\langle \beta AgInTe_2 \rangle \rightleftarrows \langle \alpha AgInTe_2 \rangle + \langle \alpha AgIn_5Te_8 \rangle \quad \text{at } 410°C$$

Table 7
Phase equilibria in the regions contained in the section at 56.7 at.% Te

Region number	Phases
1	L
2	$L + Ag_{1.9}Te$
3	$L + Ag_{1.9}Te + Ag_5Te_3$
4	$L + Ag_5Te_3$
5	$L + Ag_5Te_3 + Te$
6	$L + AgInTe_2 + Te$
7	$L + Ag_{1.9}Te + AgInTe_2$
8	$L + AgInTe_2$
9	$L + AgIn_5Te_8$
10	$L + AgIn_5Te_8 + AgInTe_2$
11	$AgInTe_2 + Ag_5Te_3 + Te$

6. Conclusion

The Ag–In–Te ternary system is characterized by the existence of the Ag_2Te–In_2Te_3 quasi-binary section. This section divides the ternary system in two independent subsystems: the triangle Ag_2Te–In_2Te_3–Te, which is the purpose of this study, and the quadrilateral Ag–Ag_2Te–In_2Te_3–In which will be the purpose of a further paper [7].

In the triangle are found three ternary compounds, which are situated in the quasi-binary section Ag_2Te–In_2Te_3. The first one, $AgInTe_2$, undergoes a peritectic decomposition at 650°C:

$$\langle AgInTe_2 \rangle \rightleftarrows \text{Liq. } p_3 + \langle AgIn_5Te_8 \rangle$$

The second one, $AgIn_5Te_8$, melts congruently at 725°C. The third one, $Ag_3In_{97}Te_{147}$ undergoes a peritectic decomposition at 672°C:

$$Ag_3In_{97}Te_{147} \rightleftarrows \text{Liq. } p_2 + \langle AgIn_5Te_8 \rangle$$

The triangle Ag_2Te–In_2Te_3–Te is divided into two sub-ternary systems: Ag_2Te–$AgIn_5Te_8$–Te and $AgIn_5Te_8$–In_2Te_3–Te.

The first sub-ternary system is formed by four invariant triangles: (1) $AgInTe_2$–AgTe–$Ag_{1.9}Te$; (2) $AgInTe_2$–$Ag_{1.9}Te$–Ag_5Te_3; (3) $AgInTe_2$–Ag_5Te_3–Te; (4) $AgInTe_2$–Te–$AgIn_5Te_8$.

The second sub-ternary system is formed by three invariant triangles: (1) $AgIn_5Te_8$–Te–$Ag_3In_{97}Te_{147}$; (2) $Ag_3In_{97}Te_{147}$–Te–In_2Te_5; (3) $Ag_3In_{97}Te_{147}$–In_2Te_5–In_2Te_3.

The eight ternary invariant points, two eutectic points, five transitory peritectic points and one metatectic point, are localized in composition and in temperature. These invariant points are found near the two In_2Te_3–Te and Ag_2Te–Te edges. They define a large crystallization area for the $AgIn_5Te_8$ congruent melting compound.

No ternary liquid–liquid miscibility gap and no glassy region are identified.

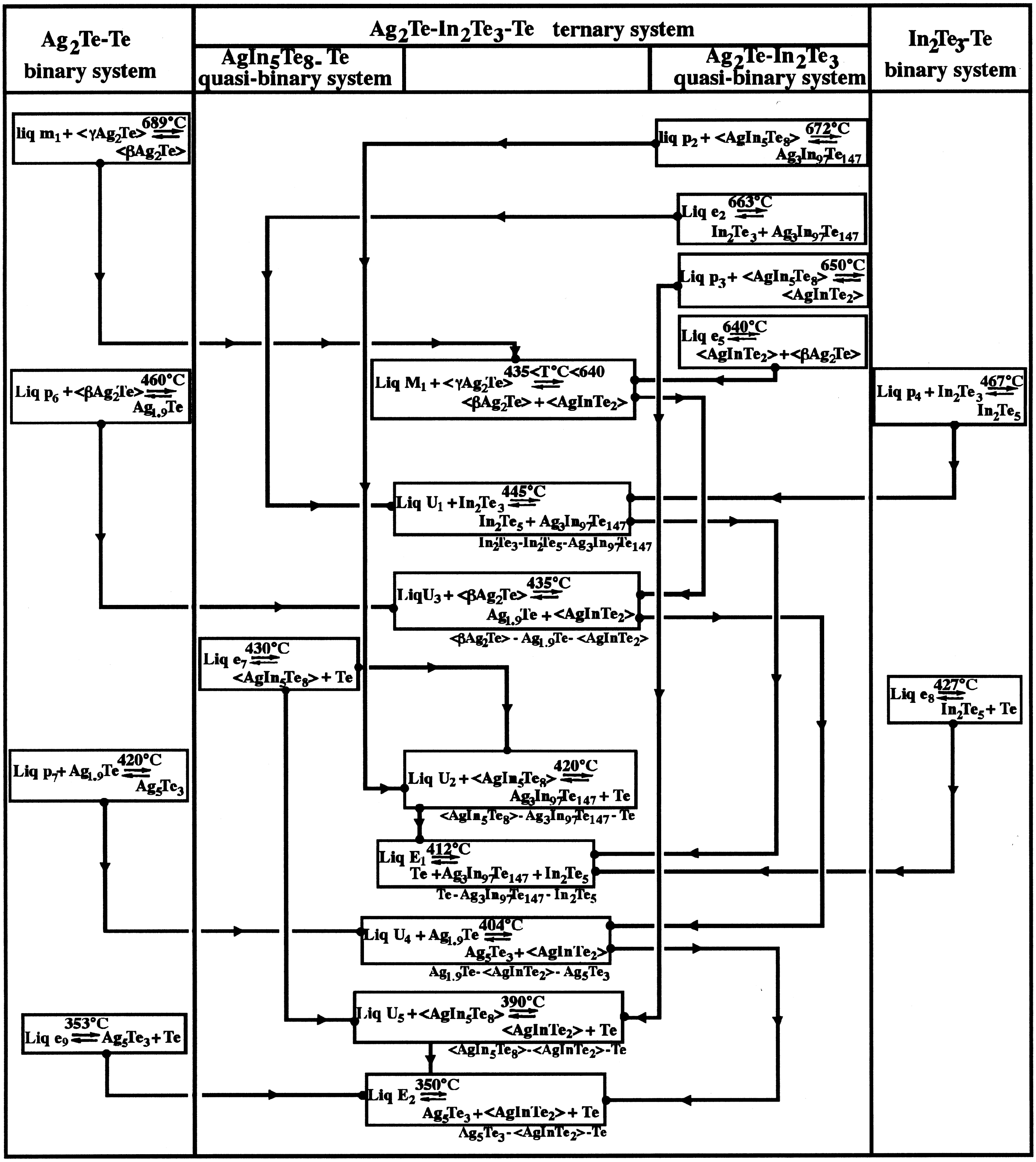

Fig. 14. Liquid–solid equilibria in the Ag_2Te–In_2Te_3–Te system.

Acknowledgements

The authors are indebted to Dr S.A. Thorén for his kind assistance with English-writing.

References

[1] M. Guittard, J. Rivet, F. Alapini, A. Chilouet, A.-M. Loireau-Lozac'h, J. Less-Common Metals 170 (1991) 373–392.

[2] A. Ferhat, R. Ollitrault-Fichet, J. Rivet, J. Alloys Compounds 177 (1991) 337–355.
[3] R. Ollitrault-Fichet, J. Rivet, J. Flahaut, C. El Kfouri, J. Solid State Chem. 110 (1994) 80–91.
[4] P.W. Chiang, D.F. O'Kane, D.R. Mason, J. Electrochem. Soc. 114 (1967) 759–760.
[5] F. Mayet, P. Roubin, CR Acad. Sci. Paris C291 (1980) 291–294.
[6] L.S. Palatnik, E.I. Rogacheva, Izv. Akad. Nauk. SSSR. Neorg. Mater. 4 (1968) 352–356.
[7] Z. Bahari, J. Rivet, B. Legendre, J. Dugué, manuscript in press.
[8] F.C. Kracek, C.J. Ksanda, L.J. Cabri, Am. Mineral. 51 (1966) 14–28.
[9] E.G. Grochowski, D.R. Mason, A.G. Schmitt, H.P. Smith, J. Phys. Chem. Solids 22 (1964) 551–558.
[10] Z. Bahari, J. Rivet, J. Dugué, CR Acad. Sci. Sér. IIc 1 (1998) 411–415.
[11] W. Guertler, Met. Erz. 85 (1920) 192.